Composition and orientation dependence of the O *K* and Fe $L_{2,3}$ EELS fine structures in $Ca_2(Al_xFe_{1-x})_2O_5$

A. Gloter
Laboratoire de Physique des Solides, UMR 8502 Bat. 510, Université Paris Sud, 91405 Orsay, France

J. Ingrin
Laboratoire d'Etude des Mécanisme des Transfert en Géologie, UMR 5563, Minéralogie, 39 Allée Jules Guesdes, 31000 Toulouse, France

D. Bouchet
Laboratoire de Physique des Solides, UMR 8502, Bat. 510, Université Paris Sud, 91405 Orsay, France

C. Colliex
Laboratoire de Physique des Solides, Bat. 510, UMR 8502, Université Paris Sud, 91405 Orsay, France and Laboratoire Aimé Cotton, UPR 3311, Bat. 505, Université Paris Sud, 91405 Orsay, France
(Received 19 March 1999)

Oxygen *K* edge and iron $L_{2,3}$ edges electron-energy-loss spectra have been collected on brownmillerites $[Ca_2(Al_x,Fe_{1-x})_2O_5]$ synthesized with different Al/Fe compositions ($0<x<0.67$). The intensity of the prepeak in the O *K* edge is directly correlated with the proportion of Fe-O-Fe bonds present in the brownmillerite. The effect of natural linear dichroism on Fe $L_{2,3}$ edges in these compounds has been evaluated together with its possible influence on the determination of the Fe $3d$-band occupation. These results have been used as a reference for the study of the Fe $2p$ spectra in Si and Ti substituted brownmillerites, which are present on a nanometer scale in cements. They demonstrate that substitution by tetravalent cations into brownmillerite is not accompanied by a significant reduction of the valence of the iron atoms. This suggests that charge compensations operate through the increase of oxygen content in the structure.

I. INTRODUCTION

Oxides with a crystallographic structure based on a perovskite basis have been extensively investigated in material science. They have attracted the ever growing attention of physicists and chemists as a consequence of their spectacular properties in many different fields, such as high-temperature superconductivity,[1] ionic conductivity,[2] and ferroelectric and ferroelastic properties,[3] accompanied by possible applications as various sensors, catalysts, and solid fuel cells.[4]

Iron-containing perovskitelike compounds are also encountered in mineralogical materials, as a main component of the earth deep interior,[5,6] but also as a major mineral phase called brownmillerites,[7] in cements. Brownmillerites may constitute as much as 40% of the cement, and generally cover a large domain of composition within the solid solution $Ca_2(Al_xFe_{1-x})_2O_5$, with numerous possible substitutions by other cations, such as titanium, silicon, and chromium. Recently, a variety of materials isostructural with brownmillerite have demonstrated a high capability to produce efficient oxygen ion conductors.[8]

The $CaMO_{2.5}$ brownmillerite structure can be described as a $CaMO_3$ perovskite structure with one-sixth of the anion sites vacant. The oxygen vacancies order in chains along the [100] direction, leading to a structure composed of alternate layers of corner-sharing MO_6 octahedra and chains of MO_4 tetrahedra stacked along [001], where *M* is a cation other than Ca.[9–11] The octahedral sites show a small distortion along the [001] direction; the metal-oxygen bonds which lie within the octahedral layer [plane (001)] are slightly shorter than those which are almost perpendicular to the layer (along [001]). The $Ca_2(Al_xFe_{1-x})_2O_5$ system constitutes a continuous solid solution from $x=0$ up to $x=0.67$. A small structural change involving the relative symmetry of tetrahedral chains between each successive layers takes place around $x=0.25$, changing from the $Ib2m$ brownmillerite symmetry above $x=0.25$ to the *Pnam* symmetry below $x=0.25$.[10] For all compositions within the $Ca_2(Al_xFe_{1-x})_2O_5$ domain, the oxide is a *G*-type antiferromagnetic insulator.[12]

During the manufacturing of cement, impurities are introduced in brownmillerite. By this way, one-fourth of the trivalent iron and aluminum ions can be replaced by tetravalent ions like Ti^{4+} and Si^{4+}. The mechanism of charge compensation accompanying the substitution of tetravalent ions into the brownmillerite structure is still a matter of debate. On one hand, Pokholov *et al.*[13] assumed that the introduction of tetravalent Sn^{4+} impurities into a synthetic $Ca_2Fe_2O_5$ leads to a change in the $3d$ electronic configuration i.e., to the creation of Fe^{2+} ions. On the other hand, Grenier *et al.*,[14] studying the $CaTiO_3$-$Ca_2Fe_2O_5$ system, and Wang *et al.*,[15] studying the related $SrTiO_3$-$Sr_2Fe_2O_5$ system, argued that the charge compensation, accompanying the replacement of iron by tetravalent Ti^{4+} involves a gradual change in the number of oxygen vacancies from the ideal perovskite structure to the brownmillerite structure. In others words, the Ti-substituted brownmillerite would have less than one-sixth of its anion sites left unoccupied, as compared to the perovskite

structure. Steinsvik *et al.*[16] proposed that the introduction of iron in the $SrTi_{1-x}Fe_xO_{3-y}$ perovskite leads to the creation of extra holes of O $2p$ character for high oxygen partial pressure (pO_2), and to the creation of oxygen vacancies for lower pO_2, suggesting that the mechanism of charge compensation may change with pO_2 conditions. In cements, like in numerous studied perovskite-like materials,[14–16] brownmillerite appears as submicronic phases, and even sometimes as nanometer-scale precipitates, requiring the use of highly spatially resolved spectroscopies. In this case, electron-energy-loss spectroscopy (EELS) attached to a transmission electron microscope (TEM), provides a unique tool to investigate the bonding of materials. In EELS, incident fast electrons cause the ionization of atoms through the ejection of a core electron resulting in an absorption edge, comparable in some conditions with those observed in x-ray-absorption spectroscopy (XAS). Then EELS provides a nanometer-scale spectroscopy of the unoccupied electron states,[17] allowing, for instance, the study of the iron d band occupation in 10-nm-wide crystals.

In this paper, we report a systematic study of the evolution of O K and Fe $L_{2,3}$ edges in reference brownmillerites $Ca_2(Al_xFe_{1-x})_2O_5$ synthesized with different Al/Fe compositions ($x=0-0.67$), and free of any tetravalent substituted cations. In particular, the effect of natural linear dichroïsm on Fe $L_{2,3}$ edges in these components has been evaluated. These results have been used as a reference for the study of Fe $2p$ spectra in Si- and Ti-substituted brownmillerites, present at a submicrometer scale in cements, in order to evaluate the existence or absence of extra electron induced in the first affinity state of the iron ion.

II. EXPERIMENTAL DETAILS AND TECHNIQUES

A set of the synthetic brownmillerite $Ca_2(Al_xFe_{1-x})_2O_5$ with a composition covering the entire range of the solid solution ($x=0$, $\frac{1}{6}$, $\frac{1}{3}$, $\frac{1}{2}$, 0.6, and 0.67) has been investigated. Samples were prepared from powder mixtures of $CaCO_3$, Al_2O_3, and Fe_2O_3 (Prolabo purity) homogenized in a ring mortar of tungsten carbide and fired at 1420 K in air for 10 h. Grinding and heating processes were performed three times in order to produce an homogeneous material. The brownmillerite structure of the samples was checked by x-ray diffraction, and no additional phase was detected. Specimens for TEM were prepared from crushed polycrystalline samples deposited on holey carbon film grids. During EELS experiments, the analyzed areas were systematically checked by selected area electron diffraction and by energy dispersive x-ray spectroscopy in order to confirm their brownmillerite structure and their suitable chemical composition. Cement samples were dryly grounded by the tripod polishing method,[18] and final thinning was achieved by argon ion milling within less than 15 min.

EELS spectra were collected in a TOPCON 002B microscope (LaB_6 gun, 200 KeV) working in diffraction mode with a $2\alpha=11$ mrad illumination angle and a $2\beta=36$ mrad collection angle. As throughout this paper small fine-structure changes are investigated, we have paid special attention to correct gain variations of the photodiode array. For the O K and Fe $L_{2,3}$ edges, at least ten shifted spectra were systematically collected, aligned, and then added. Furthermore, as anisotropy has been evidenced on Fe $L_{2,3}$ absorption edges, ''isotropiclike spectra'' have been built by adding at least ten Fe $L_{2,3}$ edges with random crystallographic orientations. When it was necessary, the crystal orientation was identified by indexing zone axis diffraction pattern. For experiments performed with these orientations, we have systematically verified through tilting the sample by few degrees that channeling effects do not significantly affect the collected EELS spectra.

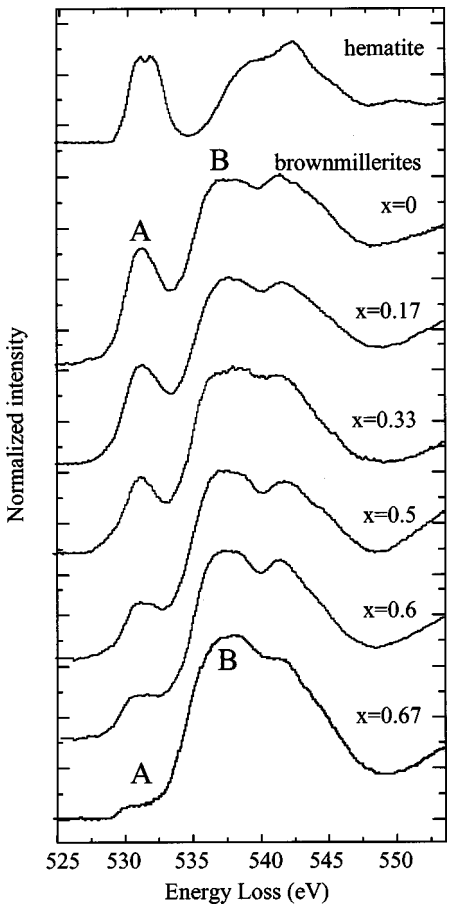

FIG. 1. Oxygen K-edge EELS spectra of α-Fe_2O_3 hematite and $Ca_2(Al_x,Fe_{1-x})_2O_5$ for various x values. Brownmillerite and hematite spectra have been normalized by keeping constant the integral of edges intensity between 527 and 548 eV.

III. RESULTS AND DISCUSSIONS

A. $Ca_2(Al_xFe_{1-x})_2O_5$ brownmillerites

1. O K edges

EELS O K-edge spectra of $Ca_2(Al_xFe_{1-x})_2O_5$ as a function of Al content are shown in Fig. 1, and can be compared with the O K spectrum of hematite (α-Fe_2O_3) recorded with the same experimental conditions (Fig. 1). Feature A; which appears as a prepeak at 531 eV, systematically decreases with the increase of Al content. This feature is attributed to unoccupied bands of primary O $2p$–Fe $3d$ character, according to previous XAS and EELS experiments and multiple-scattering calculations performed on iron-rich oxides.[16,19,20] Wu *et al.*[21] in α-Fe_2O_3, and Abbate *et al.*[20] in $LaFeO_3$, showed a splitting of the prepeak, which they interpreted as

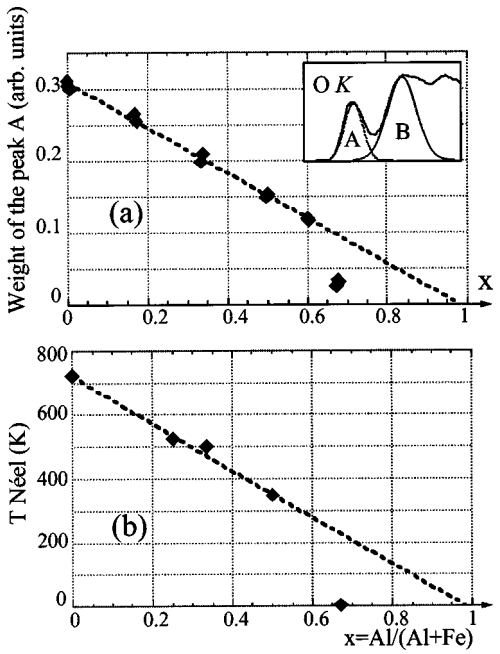

FIG. 2. Influence of Al content in brownmillerite on (a) the weight of the prepeak in the O 1*s* spectrum. A linear fit for the values $0<x<0.60$ is shown. (b) The Néel temperatures measured in Ref. 23. A linear fit for values <0.5 is also shown.

due to a difference between the energy levels of the t_{2g} and e_g orbitals induced by the crystal field. We have observed no splitting on the prepeak of brownmillerite spectra, although we could resolve such a weak splitting on the O *K* edge of hematite. This suggests that the splitting is probably smaller in brownmillerite, or that the multiplicity of the oxygen sites in brownmillerite induces a blurring effect.[19,21]

In order to estimate the relative weight of this prepeak, the *A* and *B* features were decomposed through a nonlinear fitting algorithm using two Gaussian components [Fig. 2(a)]. The integral of Gaussian *A* was divided by the integral previously used for the normalization of the spectra (the integral of the edge between 527 and 548 eV). When this ratio is plotted as a function of *x* in Fig. 2(a), it exhibits a nearly linear correlation between the weight of peak *A* and the Al content. It is only for the final value of $x(x=0.67)$ that the plot deviates strongly from the linear correlation. The general shape of the correlation is not related to the choice made to measure the weight of the prepeak. We have tried several other plots such as feature *A*/feature *B*, maximum height of feature *A*/weight of the first 20-eV integrated counts ratio; all plots show a linear behavior like that of Fig. 2(a).

The ground-state wave function can be written as

$$\Phi_G=\alpha|d^5\rangle+\beta|d^6\underline{L}\rangle,$$

where $d^6\underline{L}$ denotes the ligand hole configuration. For a given value of *x*, the intensity of peak *A* in the spectrum, which is proportional to β^2, is a measure of the covalency in the ground state.[21,22]

The linear correlation, and the fact that the fit line intersects the abscissa axis almost for $x=1$, demonstrate that the weight of the prepeak is straightly related to the iron content of brownmillerite, at least for $x<0.6$. So, we may infer that between $x=0$ and 0.6, the covalency of the Fe-O bonds is

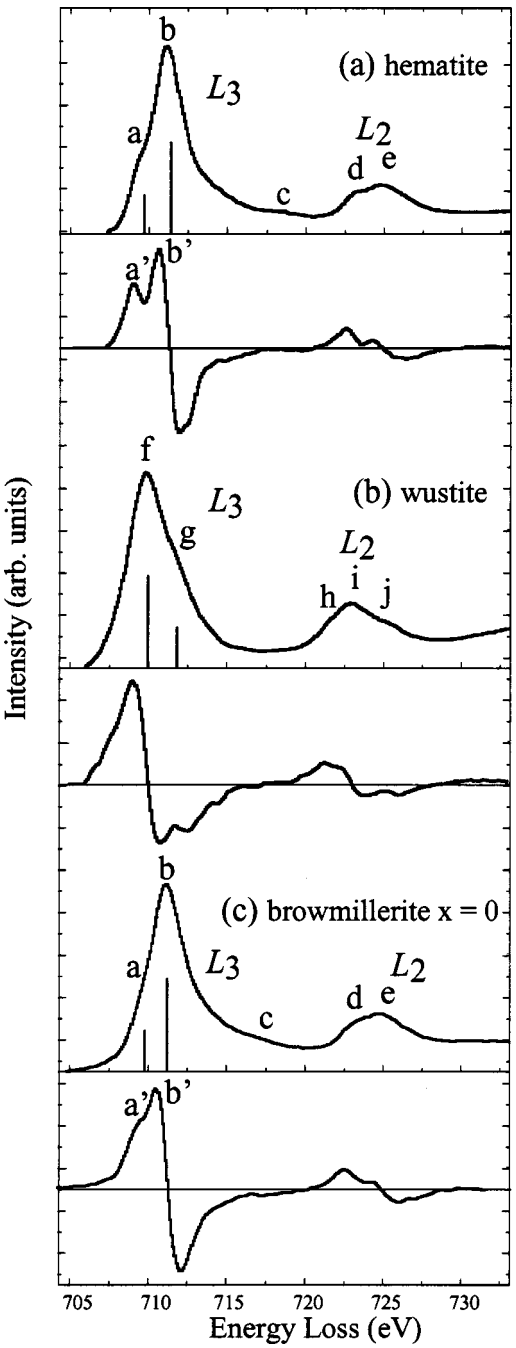

FIG. 3. Comparison between the Fe $2p$ EELS spectrum of (a) hematite, (b) wüstite, and (c) $\mathbf{x}=0$ brownmillerite. The first derivative spectra are also shown in order to emphasize the fine-structure difference between the three compounds.

probably nearly constant and almost independent on the type of sites where iron is located. Conversely, brownmillerite with an $x=0.67$ composition shows a noticeable decrease of the prepeak intensity, suggesting that Fe-O bonds become less covalent than in Al poorer compounds.

This deviation for the Al-richer brownmillerite does not arise from a change in the iron valence, since our EELS spectra (see the Fe $L_{2,3}$ edge in Fig. 3), as well as previous Mössbauer spectroscopic studies,[23] have shown only trivalent iron in $Ca_2(Al_xFe_{1-x})_2O_5$ solid solutions. The evolution of the coordination number of iron may also not be the origin of the $x=0.67$ more ionic character. Between $x=0$ and 0.67,

the average coordination of iron increases continuously from 5 to 5.6,[11,23] but no change in covalency is detected between $x=0$ and 0.6 brownmillerite, and, consequently, none would be expected for $x=0.67$ compound. Furthermore, the difference in the $d^6\underline{L}$ weight in the ground state between the tetrahedral trivalent FeO_4 cluster and the octahedral FeO_6 cluster has been estimated to be weak (around 10% for the two different coordinated sites in Fe_3O_4 magnetite[24]).

The deviation for the Al-rich compounds could arise from a change in the coordination shell around oxygen ions, i.e., the way oxygen is bridged to Al and Fe. As far as occupation factors of the different sites are concerned, the main difference of the $x=0.67$ brownmillerite is the higher occupation factor of the octahedral site. For that composition, nearly half of the octahedral sites are occupied by Al, while 80% of the tetrahedral sites are occupied by Al. Partial ordering in the (Al, Fe) solid solution would lead to the substitution of all the Fe-O-Fe bridges by Fe-O-Al bridges. In order to support this assumption, in Fig. 2(b) we plot the Néel temperature T_N of brownmillerite as a function of x.[23] Aluminum, being diamagnetic, does not participate in the superexchange interaction. Hence the substitution of Al-O-Fe bonds to the detriment of the Fe-O-Fe bonds causes the lowering of T_N. It is noticeable that T_N also vanishes for $x=0.67$ value, collapsing from 300 to 5 K within a small Al/Fe variation. According to previous Mössbauer experiments, this occurs rightly because this composition is below the percolation threshold of a Heinsenberg antiferromagnet, i.e., $(FeO_4)^{5-}$ and $(FeO_6)^{9-}$ clusters are only surrounded by Al diamagnetic ions.[23] We may infer from the similarities between Figs. 2(a) and 2(b) that the singularity in the O K edge of the Al-richer brownmillerite also originates from that percolation threshold. Iron atoms have a much more ionic ground state because the O atom does not bridge them to another iron atom. A similar variation of the ionicity, induced by a nonlocal effect, has been shown for other transition metal oxides (Ni and Cu).[25] Hu *et al.*[25] suggested that cation order between Li and Ni into $Nd_2Li_{0.5}Ni_{0.5}O_4$ results in an isolated NiO_6 clusters and to a more localized ground state compared to the $(La, Sr)_2NiO_4$ structure, where NiO_6 polyhedra are interconnected.

2. Isotropic Fe $L_{2,3}$ edge

Figures 3(a), 3(b), and 3(c) show the Fe $L_{2,3}$-edge spectra of hematite, wüstite, and brownmillerite, respectively, with their first derivative. Hematite and wüstite spectra have been collected under the same experimental conditions as for brownmillerite, and are chosen as reference spectra of Fe^{3+} [d^5 in the high-spin (HS) ground state] and Fe^{2+} (d^6 in the HS ground state), respectively. Fe $L_{2,3}$ edges correspond to excitations from the $2p^63d^n$ Fe ground state toward the $2p^53d^{n+1}$ states, where $n=5$ for Fe^{3+} and $n=6$ for Fe^{2+}.[19,24–26] The two white-line features L_3 and L_2 are separated (due to the spin-orbit splitting of the $2p$ core hole) by about 13 eV, and the energy position of the maximum of the L_3 line for divalent iron is lowered in energy by 1.6 eV, compared to the maximum of L_3 for trivalent iron, in agreement with previous XAS and EELS experimental results.[27–36] All the different extra fine structures appearing as shoulders on the sides of the two mains L_3 and L_2 (labeled $a-j$ in Fig. 3) were earlier successfully simulated by atomic multiplet calculation assuming a crystal-field strength in the range of 1.8–2 eV for hematite and 1.9–2.1 eV for wüstite.[24–27] In order to enhance the visibility of the fine structures, the derivative spectra are also displayed in Fig. 3. We will not consider Fe $2p$ spectra of low-spin $3d^{5,6}$ iron, because Van der Laan and Kirkman[34] already demonstrated that these fine structures are notably different from those of a high-spin state.

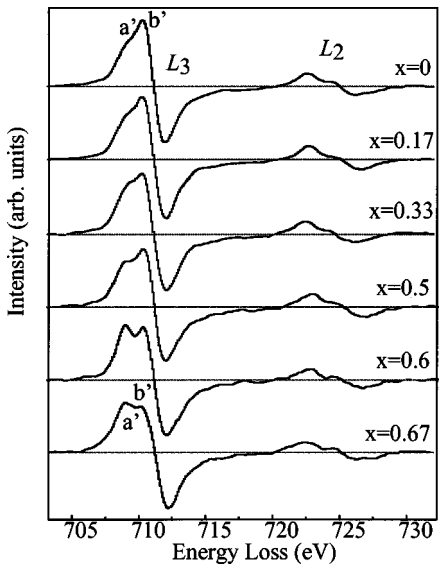

FIG. 4. Fe $2p$ EELS first derivative spectra of $Ca_2(Al_x, Fe_{1-x})_2O_5$ for various Al contents.

Qualitatively, the L_3 line of the spectrum of brownmillerite without aluminum ($x=0$; Fig. 3) compares favorably with the hematite spectrum, suggesting that the mineral is essentially composed of Fe^{3+}. Recently, two procedures[35,36] were proposed to quantify the $Fe^{3+}/\Sigma Fe$ ratio. The Garvie-Buseck[35] method, based on a decomposition of the spectrum into a linear combination of two experimentally measured spectra of end member single-valence samples, leads to a $Fe^{3+}/\Sigma Fe$ ratio of $x=0$ brownmillerite equal to 1 (taking here both hematite and wüstite measured spectra as end members). The method of Ref. 36, based on an empirical calibration of the integral intensity ratio of the L_3 line over the L_2 line (integrated on a window of 2 eV), leads to a similar value. However, this last method seems more sensitive to the white-line extraction and experimental setup, and will not be used later.

Figure 4 shows the isotropic Fe $L_{2,3}$ derivative spectra of brownmillerite with different Al contents. We report, in

TABLE I. $Fe^{3+}/\Sigma Fe$ ratio in $Ca_2(Al_x, Fe_{1+x})_2O_5$ calculated from the Garvie-Buseck method (Ref. 35).

x	$Fe^{3+}/\Sigma Fe$
0	1
$\frac{1}{6}$	1
$\frac{1}{3}$	1
$\frac{1}{2}$	1
0.6	0.97
0.67	0.91

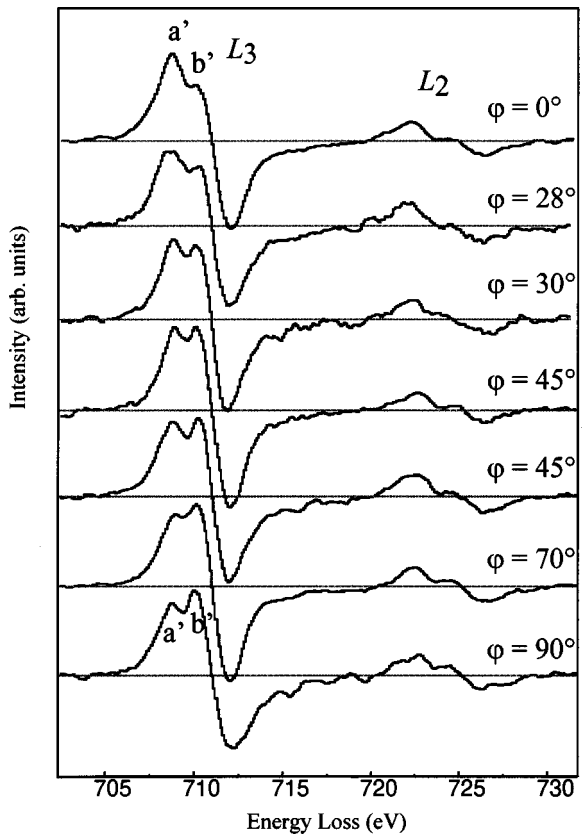

FIG. 5. Fe $2p$ EELS first derivative spectra for $x=0.67$ brownmillerite. The evolution of the a'/b' fine-structure ratio with the orientation of the crystal reflects the anisotropy due to the crystal-field interaction.

Table I, the evolution of the measured $Fe^{3+}/\Sigma Fe$, using the Garvie-Buseck method. The trivalent iron content is equal to 1 for $x<0.5$ brownmillerite. A small deviation from this value is observed for the two Al-richer samples. Nevertheless, the deviation is within the 10% reproducibility of the method.[35] This deviation observed in brownmillerite corresponds to a slight change of L_3-edge fine structure as underlined by the increase of the a'/b' ratio intensity of derivative lines (Fig. 4). As noted earlier for the O K edge, the average iron coordination in the material increases from 5 to 5.6 with Al content.[11,23] This is in agreement with the x-ray-absorption theoretical calculations of Refs. 34 and 24, showing that the tetrahedral symmetry of Fe^{3+} sites induces a higher convolution of a and b features in the L_3 line, and thus lowers the a'/b' ratio of the derivative spectrum compared to the octahedral site contribution. This may alone explain the observed deviations.

3. Orientation dependence of $x=0.67$ brownmillerite Fe $2p$ spectra

While performing the Fe $2p$ EELS measurements, we have noticed orientation effects, whose intensity increases with Al content. Figure 5 shows the evolution of the fine structures of the derivative Fe $L_{2,3}$ spectra as a function of the angle φ between the **c** axis of the brownmillerite structure and the incident electron beam, for the $x=0.67$ sample. The intensity of the a'/b' ratio is increasing, whereas φ is lowering. The observed dichroism presents an axial symmetry along **c**, and no detectable dichroism was observed along other directions. According to XAS experiments, such a dichroism may predominantly be induced either by exchange magnetic field[37–39] or by internal axial components of the crystal field (natural dichroism[40,41]). In our case, a magnetic origin for the observed dichroism may not be retained for several reasons: (i) Magnetic ordering of iron atoms is more expected for iron-rich brownmillerite ($x=0$), where each iron has an iron second-neighbor (maximum Fe-O-Fe bonds) than for iron-poor brownmillerite. (ii) The sample is subjected to the magnetic field (around 2 Te) produced by the objective lens, within the microscope. We believe that magnetic moments, for the $x=0.67$ sample, align along this external field. Then, whatever the crystallographic orientations of the sample, the magnetic moment direction should be constant. (iii) The observed increase of dichroism magnitude with the x value also suggests that octahedral iron is mainly involved in the phenomenon. In brownmillerite, octahedra are distorded toward **c** axis (Fe-O bonds are about 6.5% longer). This distortion might induce an axial component of the crystal field around the Fe ion, which is strong enough to cause anisotropic effect in EELS Fe $L_{2,3}$ edges, as already observed in some XAS experiments.[40,41]

TABLE II. $Fe^{3+}/\Sigma Fe$ ratio calculated from the Garvie-Buseck method (Ref. 35) in $x=0.67$ brownmillerite as a function of the φ angle with **c** direction.

φ(°)	$Fe^{3+}/\Sigma Fe$
0	0.95
30	0.95
45	0.95–0.91
60	0.90
62	0.84
90	0.80

An interesting practical question, raised by the dichroism observation, concerns its effect on the accuracy of quantitative methods proposed to measure ferrous/ferric ratio in nanometer-sized materials using the change in the Fe $L_{2,3}$ edge.[35,36] In Table II we report the evolution with φ angles of the $Fe^{3+}/\Sigma Fe$ ratio deduced from the Garvie-Buseck method. The specific effect of dichroism on the ferrous/ferric calculation reaches 16%.

To our knowledge, natural dichroism in transition metal $2p$ EELS spectra has not been yet reported. We discuss in more details the nature of the dichroic signal measured in TEM in Sec. III A 4.

4. Measuring EELS dichroism in a TEM configuration

In the case of dichroism in an uniaxial anisotropic material, the XAS linear dichroism is generally defined as the difference of spectra $\Delta I=I_\perp-I_\parallel$, where $I_\perp$ and $I_\parallel$ are the spectra collected with polarization perpendicular and parallel to the principal axis,[33] respectively. In the same way, for EELS transitions we can define a $I_\parallel$ spectrum, corresponding to the theoretical spectrum produced from excitations with **q**, the electron momentum transfer, parallel to the principle axis of anisotropy, here the **c** axis and a $I_\perp$ spectrum, corresponding to excitations with **q** perpendicular to **c**. In an EELS

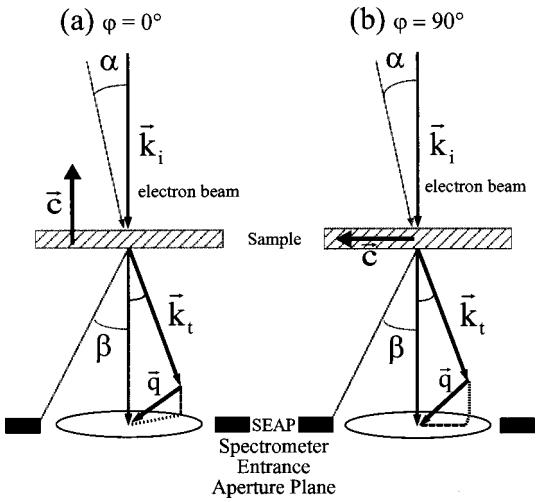

FIG. 6. Electron-scattering process for (a) the $\varphi=0°$ experiment, and (b) the $\varphi=90°$ experiment. The scattering vector **q** is the difference vector $\mathbf{q}=\mathbf{k_i}-\mathbf{k_t}$, where $\mathbf{k_i}$ is the wave vector of the 200-KeV incident electron, and $\mathbf{k_t}$ is the wave vector of the inelastically scattered electron corresponding to about 199.3 KeV since Fe$L_{2,3}$ edges are concerned. The projection of **q** parallel to **c** is plotted by the dashed line. The projection of **q** perpendicular to **c** is plotted by the dotted line.

experiment, the measured spectrum at an angle φ between **c** and the electron beam, $I(\varphi)$, is a linear combination of $I_{\parallel}$ and $I_{\perp}$. The relative weight of the two contributions depends on the experimental conditions 2α, 2β, and θ_E, where 2α is the convergence angle, 2β the collection angle, and θ_E the inelastic characteristic scattering angle. In order to illustrate this dependence, Fig. 6 shows a comparison of the scattering processes involved in the $I(\varphi=0°)$ and $I(\varphi=90°)$ experiments. From Fig. 6(a), the resulting spectrum ($\varphi=0°$) can be decomposed as

$$I(\varphi=0°)=\omega I_{\parallel}+(I-\omega)I_{\perp},$$

where ω is the proportion of transitions with **q** perpendicular to the spectrometer entrance aperture plane (SEAP here assumed perpendicular to the vertical direction; i.e., $\mathbf{q}\|\mathbf{c}$ for this geometry). We can roughly estimate ω from the integration of

$$(\vec{\mathbf{q}}\cdot\vec{\mathbf{k}}_i)^2/\mathbf{q}^2\mathbf{k}_i^2,$$

through the normalized expression

$$2\omega=\frac{\int_0^{\alpha}\sin\alpha_0\int_0^{\beta-\alpha_0}S(\theta)\dfrac{(\vec{q}\cdot\vec{k}_i)^2}{q^2\cdot k_i^2}\sin\theta d\theta d\alpha_0}{\int_0^{\alpha}\sin\alpha_0\int_0^{\beta-\alpha_0}S(\theta)\sin\theta d\theta d\alpha_0}+\frac{\int_0^{\alpha}\sin\alpha_0\int_0^{\beta+\alpha_0}S(\theta)\dfrac{(\vec{q}\cdot\vec{k}_i)^2}{q^2\cdot k_i^2}\sin\theta d\theta d\alpha_0}{\int_0^{\alpha}\sin\alpha_0\int_0^{\beta+\alpha_0}S(\theta)\sin\theta d\theta d\alpha_0} \quad (1)$$

where $S(\theta)$ is the angular distribution of inelastic scattering. The two successive integrations are accounting for the finite convergence angle of the probe and for the collection angle delimited by the spectrometer entrance aperture. Using our experimental value, i.e., $2\alpha=11$ mrad, $2\beta=32$ mrad, and $\theta_E=2.05$ mrad, and assuming that $S(\theta)=1/(\theta^2+\theta_E{}^2)$ in the dipolar approximation,[42] relation (1) gives $\omega=0.21$ for the Fe $L_{2,3}$ edge. This quantitative value of the contribution arising from $\mathbf{q}\|\mathbf{c}$ transitions in the electron energy loss is in good agreement with the value found by Menon and co-workers[43] using a different calculation method.

Figure 6(b) shows the scattering geometry for $\varphi=90°$. In this case, it leads to a measured spectrum

$$I(\varphi=90°)=\omega I_{\perp}+(1-\omega)(I_{\perp}+I_{\parallel})/2. \quad (2)$$

The first term in the right-hand side of Eq. (2) corresponds to scattering events with **q** perpendicular to the SEAP. The last term corresponds to transitions with **q** in that plane. Thus in EELS the dichroism ΔI can be written as

$$\Delta I=I(\varphi=0°)-I(\varphi=90°)=(1-3\omega)(I_{\perp}-I_{\parallel})/2, \quad (3)$$

leading to $\Delta I=0.185(I_{\perp}-I_{\parallel})$, in our experimental conditions. The resulting EELS dichroism signal is a part only of the maximum difference spectrum attainable in XAS linear dichroism ($I_{\perp}-I_{\parallel}$). Nevertheless, this effect is not negligible, and must be taken into account when quantifying Fe $2p$ EELS spectra. Equation (3) predicts conditions ($\omega=\frac{1}{3}$) corresponding to an isotropic measurement. Nevertheless, the illumination conditions required to achieve this value are inadequate for a nanometer-scale analysis, and then cannot be used.

B. Application to Ti and Si substituted brownmillerite in cement

One of the main differences between Fe-Al brownmillerites, studied above, and those which are present in cements, is the frequent partial substitution of Fe and Al by Ti and Si. The content of these tetravalent cations is highly variable with the considered crystal, and can reach 5 at. %.[44–46]

The substitution processes of tetravalent cations in brownmillerite are not fully elucidated. Two mechanisms of charge compensation have been proposed: the first one by simultaneous substitution of divalent cations (Mg^{2+},Fe^{2+}),[13,45,47] the second by addition of O^{2-}.[44] We have observed a set of several nanosized brownmillerite crystals with varying Ti+Si contents. The range of cationic composition is $Ca_1Al_{0.24-0.47}Fe_{0.45-0.61}Si_{0.07-0.14}Ti_{0.02-0.06}Cr_{0-0.003}$.[46] If considering the first proposed mechanism, the only potential divalent cations available are iron ions. Such a charge compensation, would then lead to a charge reduction of 14–44% of Fe. As we have seen above, even if we pay no attention to crystal orientation, such a large reduction may be easily detected by the mean of the Fe $2p$ spectra using the quantitative analyzes developed by Garvie and Buseck.[35] An example of the Fe $L_{2,3}$ edge [Fig. 7(a)] collected on a substituted brownmillerite [(Si+Ti)/ΣFe=0.34] can be compared with the Fe-Al brownmillerite spectra (Fig. 3). From the resulting $Fe^{2+}/\Sigma Fe$ values, which are plotted as a function of the (Si+Ti)/ΣFe ratio [Fig. 7(b)], we evaluated the average content of Fe^{2+} present in these brownmillerites to be equal to $8\%\pm5\%$. This value being in the limit of the detection method and whatever the scattering effect of dichroism due to the random orientation of the crystal, only a

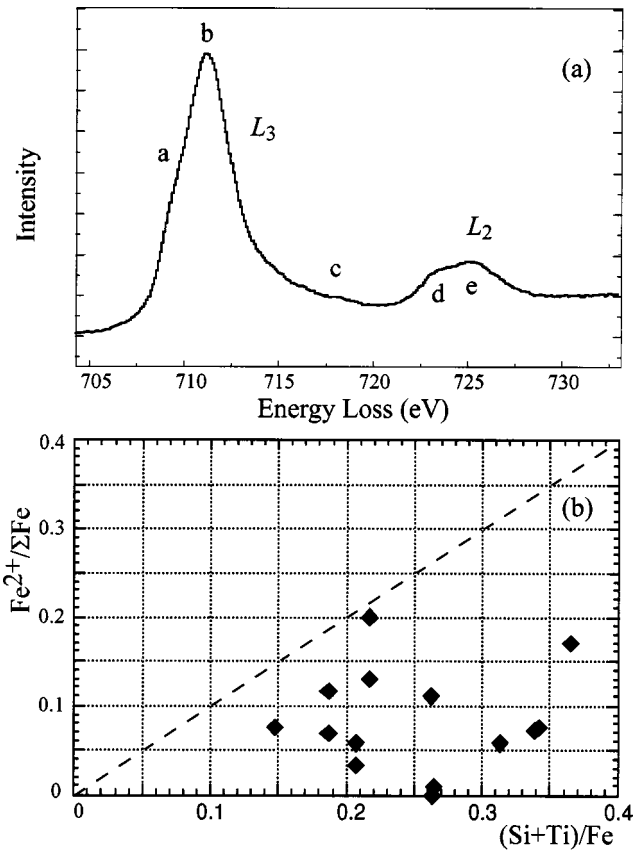

FIG. 7. (a) Fe $2p$ EELS spectrum of a brownmillerite with $(Si+Ti)/\Sigma Fe=0.34$. (b) $Fe^{2+}/\Sigma Fe$, deduced from the analyses of the Fe $L_{2,3}$ edges, as a function of the $Ti^{4+}+Si^{4+}$ content. A line with slope 1 is shown for comparison.

very small fraction (even none) of Fe seems to be reduced. Nevertheless, this amount is too low to compensate efficiently for the charge excess due to substitution. Thus charge compensation is more likely explained by the introduction of oxygen anions in the structure of brownmillerite.

IV. CONCLUSION

We have shown how EELS fine structures of O *K* and Fe $L_{2,3}$ are modified with the aluminum content in $Ca_2(Al_xFe_{1-x})_2O_5$. We have provided evidence of the similarity between the evolution of the O *K* prepeak intensity and the Néel temperature with the Al content. This suggests that this prepeak is directly correlated with the proportion of Fe-O-Fe bonds present in the brownmillerite. Smooth modifications of lines L_3 and L_2 of Fe $L_{2,3}$ edges, observed with Al increase, may be qualitatively explained by the progressive decrease of the contribution of tetrahedral iron compared to octahedral iron. Furthermore, we have shown with the EELS technique, the dichroism of Fe $2p$ spectra along the **c** axis. These last two phenomena affect the efficiency in the quantitative determination of the iron valence from the near-edge features, as recently proposed.[35,36] In the peculiar case of dichroism in brownmillerite, one can obtained a deviation from the real $Fe^{3+}/\Sigma Fe$ ratio, which can reach 16%.

When applied to highly substituted nanometer-size brownmillerite crystals occurring in cements, these techniques show that substitution by tetravalent cations such as Si and Ti is not accompanied by a significant reduction of iron. These experiments suggest that, during these substitutions, charge compensations operate through the increase of oxygen content in the structure. It has to be noted that, at the present time, no direct experimental methods are available to measure the oxygen content with the required precision, on a nanometer scale.

Orientation dependence of Fe $L_{2,3}$ spectra demonstrate that EELS spectra are sensitive to the ground-state splitting induced by an axial crystal field. Then high spatially resolved EELS appears as a promising technique for the study of other systems, such as interfaces, thin films, and multilayers where local anisotropy of crystal field is significant and of great interest. Furthermore, the recent work of Menon and Yuan,[48] demonstrating the phenomenon of magnetic linear dichroism in EELS, strengthen this assumption.

ACKNOWLEDGMENTS

This work received financial support from the LAFARGE Company and the ANRT organization under a Cifre Contract for one of us (A.G.). We are pleased to thank O. Stephan for stimulating discussions and for her suggestions.

[1] M. K. Wu, J. R. Asburn, C. J. Torng, C. J. Hor, R. L. Meng, L. Gao, Z. J. Huang, Y. K. Wang, and C. W. Chu, Phys. Rev. Lett. **58**, 908 (1987).
[2] S. Shin, M. Yonemura, and H. Ikawa, Mater. Res. Bull. **XIII**, 1017 (1978).
[3] I. P. Aleksendrova, B. S. Bagautdinov, J. Bartolone, R. Burniel, J. I. Melero, M. A. Popov, and S. V. Primak, Ferroelectrics **115**, 169 (1995).
[4] K. R. Kendal, C. Navas, J. K. Thomas, and H. C. zur Loye, Solid State Commun. **82**, 215 (1995).
[5] T. Katsura and E. Ito, Geophys. Res. Lett. **23**, 2005 (1996).
[6] C. McCammon, Nature (London) **387**, 694 (1997).
[7] K. L. Scrivener and A. Capmas, in *LEA's Chemistry of Cement*, edited by P. C. Hewlett (Anrolf, London, 1998).
[8] C. A. J. Fisher, M. S. Islam, and R. J. Brook, J. Solid State Chem. **128**, 137 (1997).
[9] A. A. Colville and S. Geller, Acta. Crystallogr., Sect. B: Struct. Crystallogr. Cryst. Chem. **27**, 2311 (1971).
[10] A. A. Colville and S. Geller, Acta. Crystallogr., Sect. B: Struct. Crystallogr. Cryst. Chem. **28**, 3196 (1972).
[11] F. Guirado, F. Sorrentino, S. Gali, and S. Chinchon, Cem. Conc. Res. **24**, 360 (1994).
[12] T. C. Gibb and M. Matsuo, J. Solid State Chem. **88**, 485 (1990).
[13] K. H. Pokholok, L. Fournes, G. Demazeau, and P. B. Fabritchnyi, Solid State Commun. **66**, 123 (1988).
[14] J. C. Grenier, G. Schiffmacher, P. Caro, M. Pouchard, and P. Hagenmuller, J. Solid State Chem. **20**, 365 (1977).
[15] Y. G. Wang, S. Steinsvik, R. Hoier, and T. Norby, J. Mater. Sci.

Lett. **14**, 1027 (1995).
[16] S. Steinsvik, R. Bugge, J. Gjonnes, J. Taftö, and T. Norby, J. Phys. Chem. Solids **58**, 969 (1997).
[17] C. Colliex, M. Tencé, E. Lefèvre, C. Mory, H. Gu, D. Bouchet, and C. Jeanguillaume, Mikrochim. Acta **114/115**, 71 (1994).
[18] J. Ayache and P. H. Albarede, Ultramicroscopy **60**, 195 (1995).
[19] C. Colliex, T. Manoubi, and C. Ortiz, Phys. Rev. B **44**, 11 402 (1991).
[20] M. Abbate, F. M. F. de Groot, J. C. Fuggle, A. Fujimori, O. Strebel, F. Lopez, M. Domke, G. Kaindl, G. A. Sawatzky, M. Takano, Y. Takeda, H. Eisaki, and S. Uchida, Phys. Rev. B **46**, 4511 (1992).
[21] Z. Y. Wu, S. Gotta, F. Jollet, M. Pollak, M. Gautier-Soyer, and C. R. Natoli, Phys. Rev. B **55**, 2570 (1997).
[22] I. Davoli, A. Marcelli, A. Bianconi, M. Tomellini, and M. Fantoni, Phys. Rev. B **33**, 2979 (1986).
[23] G. Y. Kim, K. S. Roh, and C. H. Yo, Bull. Korean Chem. Soc. **16**, 934 (1995).
[24] J. P. Crocombette, M. Pollack, F. Jolet, N. Thromat, and M. Gautier-Soyer, Phys. Rev. B **52**, 3143 (1995).
[25] Z. Hu, C. Mazumbar, G. Kaindl, F. M. F. de Groot, S. A. Warda, and D. Reinen, Chem. Phys. Lett. **297**, 321 (1998).
[26] F. M. F. de Groot, J. C. Fuggle, B. T. Thole, and G. A. Sawatzky, Phys. Rev. B **42**, 5459 (1990).
[27] G. Cressey, C. M. B. Henderson, and G. van der Laan, Phys. Chem. Miner. **20**, 111 (1993).
[28] L. A. J. Garvie, A. C. Craven, and R. Brydson, Am. Mineral. **79**, 411 (1994).
[29] Th. Cshedel-Niedrig, W. Weiss, and R. Schlogel, Phys. Rev. B **52**, 17 449 (1995).
[30] J. van Elp, G. Peng, Z. H. Zhou, S. Mukund, and M. W. W. Adams, Phys. Rev. B **53**, 2523 (1996).
[31] H. Wang, G. Peng, L. M. Miller, E. M. Scheuring, S. J. George, M. R. Chance, and S. P. Cramer, J. Am. Chem. Soc. **119**, 4921 (1997).
[32] T. Uozumi, K. Okada, A. Kotani, R. Zimmerman, P. Steiner, S. Hufner, Y. Tezuka, and S. Shin, J. Electron Spectrosc. Relat. Phenom. **83**, 9 (1997).
[33] P. F. Schofield, G. van der Laan, C. M. B. Henderson, and G. Gressey, Miner. Mag. **62**, 65 (1998).
[34] G. van der Laan and I. W. Kirkman, J. Phys.: Condens. Matter. **4**, 4189 (1992).
[35] L. A. J. Garvie and P. R. Buseck, Nature (London) **396**, 667 (1998).
[36] P. A. van Aken, B. Liebscher, and V. J. Styrsa, Phys. Chem. Miner. **25**, 323 (1998).
[37] G. van der Laan and B. T. Thole, Phys. Rev. B **43**, 13 401 (1991).
[38] P. Rudolf, F. Sette, L. H. Tjeng, G. Meigs, and C. T. Chen, J. Magn. Magn. Mater. **109**, 109 (1992).
[39] P. Kuiper, B. G. Searle, P. Rudolf, L. H. Tjeng, and C. T. Chen, Phys. Rev. Lett. **70**, 1549 (1993).
[40] M. Sacchi, O. Sakho, and G. Rossi, Phys. Rev. B **43**, 1276 (1991).
[41] G. van der Laan, P. F. Schofield, G. Gressey, and C. M. B. Henderson, Chem. Phys. Lett. **252**, 272 (1996).
[42] R. F. Egerton, *Electron Energy Loss Spectroscopy in the Electron Microscope*, 2nd ed. (Plenum, New York, 1996).
[43] N. K. Menon and J. Yuan, Ultramicroscopy **74**, 83 (1998); N. K. Menon, Ph.D. thesis, University of Cambridge, 1998.
[44] M. B. Marinho and F. P. Glasser, Cem. Conc. Res. **14**, 360 (1984).
[45] I. G. Richardson, C. Hall, and G. W. Groves, Adv. Cem. Res. **5**, 15 (1993).
[46] A. Gloter, J. Ingrin, D. Bouchet, K. L. Scrivener, and C. Colliex, Phys. Chem. Miner. (to be published).
[47] T. B. Berstrom, C. Hall, and K. L. Scrivener, Adv. Cem. Res. **4**, 141 (1991).
[48] N. K. Menon and J. Yuan, Ultramicroscopy **78**, 185 (1999).